Stesmans et al. Nanoscale Research Letters (2017) 12:283
DOI 10.1186/s11671-017-2008-x

Nanoscale Research Letters

NANO EXPRESS Open Access

Paramagnetic Intrinsic Defects in Polycrystalline Large-Area 2D MoS_2 Films Grown on SiO_2 by Mo Sulfurization

A. Stesmans[1*], S. Iacovo[1], D. Chiappe[2], I. Radu[2], C. Huyghebaert[2], S. De Gendt[2] and V. V. Afanas'ev[1]

Abstract

A low-temperature electron spin resonance study has been carried out on large-area high-purity polycrystalline two-dimensional few monolayer (ML) 2H MoS_2 films synthesized by sulfurization of Mo layers, with intent to atomically assess mobility-degrading detrimental point defects. This reveals the presence of a distinct previously unreported anisotropic defect of axial symmetry about the *c*-axis characterized by $g_{//} = 2.00145$ and $g_{\perp} = 2.0027$, with corresponding density (spin S = ½) ~3×10^{12} cm^{-2} for a 4 ML thick film. Inverse correlation of the defect density with grain size points to a domain boundary associated defect, inherently incorporated during sample growth. Based on the analysis of ESR signal features in combination with literature data, the signal is tentatively ascribed to the a (di)sulfur antisite defect (S or S_2 substituting for a Mo atom). Beset by these defects, the grain boundaries thus emerge as an intolerable threat for the carrier mobility and layer functionality.

Keywords: Large-area 2D molybdenum disulfide, Synthetic 2D molybdenum disulfide, Point defects, Intrinsic defects, Grain boundaries, Electron spin resonance

Background

Next to graphene, MoS_2 is touted as a post-Si semiconductor that may revolutionize electronics because of distinct advantages [1–3]. Unlike graphene, a two-dimensional (2D) MoS_2 monolayer (ML) is a 1.85-eV direct bandgap semiconductor [4], which makes it most appropriate for integrated logic and optoelectronic applications. The practical realization of any of these will require synthesis of large-area high-quality 2D MoS_2 layers, stimulating research for optimal production techniques [5, 6].Yet, related with the growth process, inevitably present structural defects, such as point defects and grain boundaries, manifestly degrade the performance, including electrical mobility degradation to values still one or two orders of magnitude below the theoretical one of ~410 cm^2/Vs for electrons [1, 5, 7–9]. Many kinds of intrinsic point defects have been theoretically [5, 10–15] and experimentally [5, 11, 16] assessed including vacancies, antisites, and interstitials, with the sulfur vacancy, V_S—an acceptor [10, 17]—emerging with the lowest formation energy [5, 10, 11]. Using high-resolution scanning transmission electron microscopy (STEM) techniques, several defects have been experimentally "visualized" [5, 11, 16] and their occurrence statistically analyzed [5].

Obviously, adequate steering of the realization of high-quality 2D crystalline films requires, besides identification, also quantification of the various type defects before these can put under control. In an exploring approach, the current work deals with high-purity large-area 2D MoS_2 polycrystalline layers synthesized by sulfurization of Mo films, focusing on occurring detrimental point defects with the intent to atomically assess and quantify these by means of electron spin resonance (ESR), an exclusive tool for that purpose. A pristine signal, of substantial intensity, is revealed, suggested to originate from a native defect related with grain boundaries, thus unveiling a severe threat to performance.

Methods

The starting sample substrates were 2 cm × 2 cm two-side polished Cz-(100)Si slices (B-doped; ~1 Ω cm; ~100 μm thick) thermally oxidized (~50 nm thick) at

* Correspondence: andre.stesmans@fys.kuleuven.be
[1]Department of Physics and Astronomy, University of Leuven, 3001 Leuven, Belgium
Full list of author information is available at the end of the article

both sides, and subsequently subjected to heating in H_2 (1 atm; 6 N pure; 430 °C) to ESR-inactivate the inevitable interfacial Si dangling bond (DB) defects (P_b-type centers) [18]. On these substrates, a thin Mo layer with thickness in the range 0.2–0.5 nm, as measured by quartz monitored weighing, was sputtered at a deposition rate of 0.01 nm/s from a high-purity Mo source in high vacuum, followed by MoS_2 layer synthesis through sulfurization at 800 °C for 30 min in pure H_2S at a pressure p_{H2S} of 100 mbar (process a) or 10 mbar (process b), according to the chemical reaction $Mo + 2H_2S \rightarrow MoS_2 + 2H_2$ (*g*). As exposed by STEM analysis, this resulted in continuous large-area 2D MoS_2 polycrystalline films, with ~20–40 nm sized grains, in the 2H phase (hexagonal symmetry, two MoS_2 layers per repeat unit, and Mo in trigonal prismatic coordination; D_{3h} point group). This is illustrated in Fig. 1, showing a plane-view STEM image of a large area MoS_2 film obtained by sulfurization process a, the layer being characterized by an average grain size of ~20 nm across. Cross-sectional TEM observations show that film thicknesses of up to 4 MLs, rather uniform, are obtained with the molecular planes preferentially aligned parallel to the SiO_2 substrate surface. More details about the synthesis, morphological and structural analysis, and performance can be found elsewhere [19].

Three samples were examined: a first with one MoS_2 monolayer (1MLa) grown at $p_{H2S} = 100$ mbar, a second 4-layer thick one (4MLa) grown at $p_{H2S} = 100$ mbar, and a third 4-layer one (4MLb) grown at $p_{H2S} = 10$ mbar. Atomic force imaging of the 4ML samples shows an increase in average grain size from ~20 to ~40 nm by reducing p_{H2S}. From measurements on bottom-gated transistors fabricated using these large-area 4ML MoS_2 films, extrinsic low-field field-effect carrier mobilities of ~0.001 and ~0.02 cm^2/Vs were obtained, respectively.

For ESR purposes, the as-received samples were mechanically cleaved into 2 mm × 10 mm slices, with their 10-mm edge along the Si [0 $\bar{1}$1] direction. In assembling an ESR sample (typically ~20 slices), full wafer coherence in crystallinity was maintained through stacking slices with their Si substrate [0 $\bar{1}$1] direction all "up" in the bundle. Defects were characterized using conventional low-temperature X, K, and Q-band ESR spectroscopy [18]. Some samples were additionally subjected to thermal treatment in vacuum ($p \leq 5 \times 10^{-6}$ mbar) at $T = 330$ °C for appropriate times.

Results

Figure 2 presents an overview of representative first-derivative (dP_μ/dB, where P_μ is the applied microwave power and **B** the magnetic field) K-band ESR spectra measured for **B** parallel to the [100] surface normal (**n**) at 1.8 K in the $g = 2.018$–1.98 range (~130 G scan) for the three types of samples studied. Two main signals are observed: The first, observed at $g \sim 2.0057$ with peak-to-peak width $\Delta B_{pp} \sim 8$G for **B**//**n** and exhibiting distinct *g* factor anisotropy (not shown), stems from the known anisotropic Si DB $P_{b0}^{(110)}$ defects at the (110)Si/SiO_2 interface, well expected from the (011) and (0$\bar{1}$1) cleavage edges of the (100)Si slices. The signal is identically

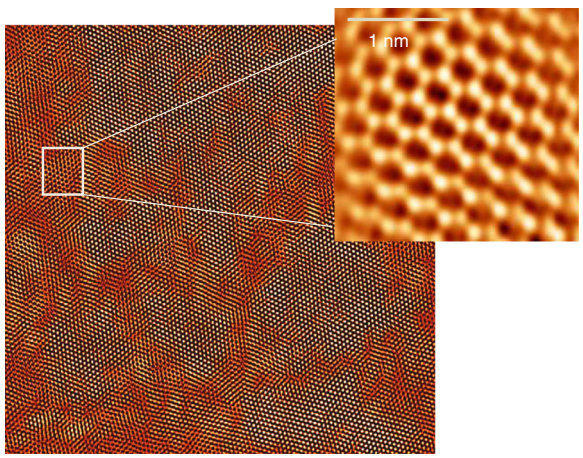

Fig. 1 Plane-view STEM image of a large-area MoS_2 film synthesized on SiO_2 by sulfurization of a predeposited (sputtered) Mo layer at 800 °C in H_2S (100 mbar; 30 min) exposing a uniform polycrystalline film of average grain size ~20 nm; The zoomed in picture shows the hexagonal structure and trigonal prismatic atomic arrangement geometry

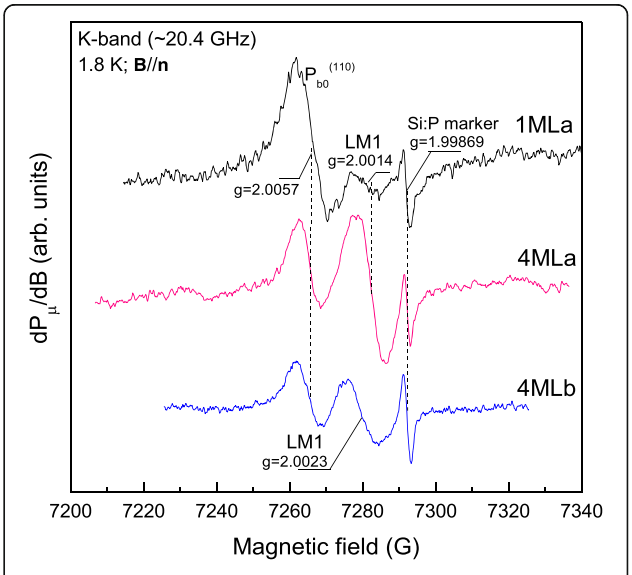

Fig. 2 K-band ESR spectra observed at 1.8 K using $P_\mu \sim 25$ nW for **B**//**n** on three 2D MoS_2/SiO_2/(100)Si entities, showing the observation of the LM1 signal (at $g \sim 2.0014$ in the process-a samples). The signal at $g = 1.99875$ stems from a co-mounted Si:P marker sample, also used for field axis alignment of the spectra. The spectra have been normalized to equal Si:P marker intensity and sample area

observed, and the only one, on a SiO_2/(100)Si/SiO_2 reference sample without MoS_2 layers on top. Of key interest is the 2nd signal of $\Delta B_{pp} \sim 7$G, labeled LM1, appearing at $g \sim 2.0014(2)$ in the process-a (1MLa, 4MLa) samples. Field angular measurements for **B** rotating in the Si $(0\bar{1}1)$ plane (**B** at angle φ_B with **n**) result in the g map shown in Fig. 3, revealing anisotropy. The map points to a defect of axial (C_{3v}) symmetry where the axial ($g_{//}$) axis is restricted to only one direction with respect to the sample morphology, i.e., parallel to the MoS_2 layer normal **n**, with potentially allowed other crystallographically equivalent defect orientations in a bulk crystal not occurring. Optimized fitting to axial symmetry yields $g_{//} = 2.00145$ and $g_{\perp} = 2.0027$.

The defect appears in substantial densities, with inferred values of $\sim 3 \times 10^{11}$ and 3×10^{12} cm^{-2} for the 1MLa and 4MLa samples, respectively. A similar signal, with corresponding density $\sim 0.8 \times 10^{12}$ cm^{-2}, is observed in the low $p_{H2S} = 10$ mbar sample 4MLb at $g \sim 2.0023$ but now behaving more isotropic. Here, we may notice that the latter value coincides with the g-matrix trace $g = (g_{//} + 2g_{\perp})/3 = 2.00228$. Within experimental accuracy, the signal remains unchanged after vacuum treatment of the sample at 330 °C for ~150 min.

As illustrated by the plot in Fig. 4 of the inverse signal intensity I (area under the absorption curve ∝ magnetic susceptibility χ) vs. T, the signal behaves almost perfectly paramagnetic [$\chi \propto T^{-1}$] within experimental uncertainty; Fitting of the Curie-Weiss law $\chi \propto (T - T^{-1})$, gives a Curie temperature $T_C = 0.5 \pm 0.5$ K, i.e., close to 0, which points to a spin system of localized defects with negligible mutual interaction. It is indicative of a defect system distributed in a dilute manner with negligible defect clustering. As the LM1 signal is not observed in the thermal SiO_2/(100)Si/SiO_2 control sample, it should originate from the 2D MoS_2 layer, and based on the high-purity level attained with synthesized MoS_2 layers, it is reasonable to ascribed it to a native intrinsic defect.

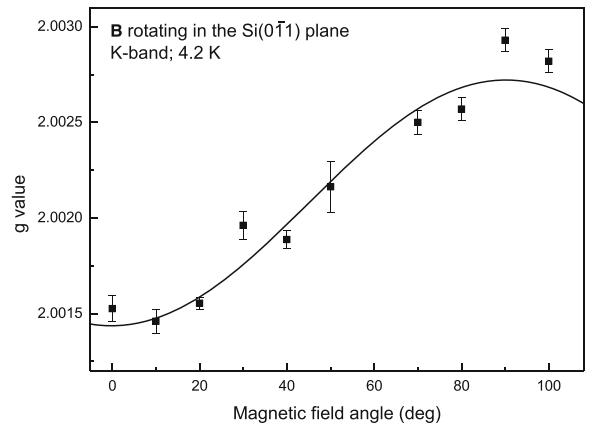

Fig. 3 g map of the LM1 defect in MoS_2 sample 4MLa inferred from K-band ESR measurements at 4.2 K for **B** (at angle φ_B with **n**) rotating in the Si substrate $(0\bar{1}1)$ plane. The solid curve represents an optimized fitting of expression $g(\varphi_B) = [g_{//}^2 \cos^2(\varphi_B) + g_{\perp}^2 \sin^2(\varphi_B)]^{1/2}$ for a center of axial (C_{3v}) symmetry giving $g_{//} = 2.00145$ and $g_{\perp} = 2.0027$

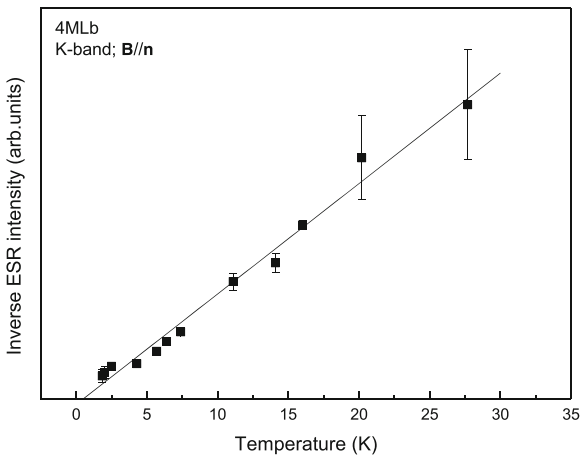

Fig. 4 Plot of the inverse ESR intensity of the LM1 signal from sample 4MLb vs temperature. The data point to a spin system behaving closely paramagnetic ($\chi^{-1} \propto T$), characterized by a Curie temperature $T_c = 0.5 \pm 0.5$ K as obtained from the optimized linear fitting (*solid line*) of the Curie-Weiss law $\chi^{-1} \propto (T - T_c)$

Discussion

Having revealed a first exclusive paramagnetic point defect pertaining to 2D MoS_2 layers, it remains to address its atomic nature. Dealing with 2D layers deposited on SiO_2/Si substrates, in search of its atomic character, there is the basic question about the location of the defect at/in the MoS_2 layers studied, for which we face several possibilities, i.e., edge defects, ad-atom (surface) centers, or "inner" layer defects. Here, as a first inference, the kind of rather high density of defects observed precludes right away, for a continuous layer, these to originate from the MoS_2 layer edges. Next, the fact that the LM1 signal is observed not to be affected by treatment in vacuum at 330 °C (~150 min), would exclude the observed signal neither to concern an ad-atom center [10]. As to its location, this thus leads us to considering a more inner layer positioned *intrinsic* defect, in which case the abundant grain boundaries emerge as primary suspect. Some independent support for this hypothesis comes from the fact that the signal is not observed by independent high-sensitivity ESR measurements on a natural as-received 2H MoS_2 crystal (not shown). The suggestion is further supported by the observed decrease in defect density for the 4MLb MoS_2 layer compared to the 4LMa one, i.e., in correlation with the increase in average grain size (~20 vs. ~40 nm), with attendant substantial reduction in amount of grain boundaries—and hence in the total of associated point defects—and drastic improvement in carrier mobility [19].

Reliable atomic identification generally would require the observation of ESR hyperfine (hf) structure, which in the current case should come from the isotopes ^{33}S (nuclear spin $I = 3/2$; 0.75% abundance) and ^{95}Mo and ^{97}Mo (both $I = 5/2$; 25.5% added abundance). Yet, despite spectroscopic realization of a signal-to-noise ratio >300 for the LM1 Zeeman signal, no clear hf structure could be resolved. Based on the involved Mo nuclear magnetic moment strength $\mu_n = g_n\beta_n I = -0.37\beta_n I$ (where g_n and β_n represent the nuclear g factor an nuclear magneton, respectively) [20] and natural isotopic abundance, this makes it unlikely the defect to concern a Mo-centered unpaired electron defect.

No previous report of an LM1-like ESR spectrum in MoS_2 could be traced in the literature. Also, based on g value considerations, literature search would indicate the signal not to originate from unsaturated sulfur atoms (radicals) or Mo atoms in the formal 5+ oxidation state [21].

Obviously, regarding intrinsic defects in the two-atom MoS_2 material, there are various possible variants. Using the annular dark-field (ADF) STEM technique, several works have recently managed atomic-scale visualization of intrinsic structural defects—point defects, dislocations, grain boundaries, edges—in MoS_2 monolayer prepared by various methods, including mechanical exfoliation [5] from natural MoS_2 samples, chemical vapor deposition [5, 11], and physical vapor deposition (PVD) [5]. There, besides the various types of vacancy centers (i.e., V_S, V_{Mo}, V_{S2}, V_{MoS3}, V_{MoS6}), eye catching was the demonstration of the presence of various antisite centers like S_{Mo} (a sulfur atom substituting for a Mo site), $S2_{Mo}$, Mo_S, and Mo_{S2}. ADF-STEM observations showed that the Mo_{S2} antisite defects, followed by Mo_S, are far dominant defects in PVD MoS_2 monolayers reaching densities of $\sim 2.8 \times 10^{13}$ cm^{-2}. Substantial densities of S_{Mo} were found in mechanically exfoliated MoS_2 monolayers. Thus, antisites have been atomically resolved in various instances [5, 11], also in connection with grain boundaries.

It has been concluded that antisites should play an important role in the dislocation and grain boundary structures [10, 14, 22]. Also, antisites are reported to have a strong effect on the phonon-limited mobility of electrons, far more drastic than V_S or V_{S2}. [5]. With these findings as background, in light of the distinct polycrystalline nature of the MoS_2 films currently studied, it is suggested the LM1 signal to originate from antisite defects associated with grain boundaries, where based on the salient ESR properties, the S_{Mo} or $S2_{Mo}$ antisites come to the fore as most likely.

If correct, then based on the observed defect density and measured average grain size, we would have ~1.5–3.5 antisite defects per 10-nm length of grain boundary. Obviously, these will drastically devastate the carrier mobility. Accordingly, this mandates that the production method is to be upgraded so as to drastically reduce their generation, or else, if unavoidably incorporated, an appropriate method should be developed that enables efficient and robust electrical inactivation (passivation) of these defects.

It should be noticed that, given the large formation energy (E_{form}) involved [14], the grain boundaries, and likely the associated antisite defects as well, come as "non-equilibrium" structures introduced by sample growth modalities and history. Their appearance is seen as inherent to the specific synthesis method, carried out at relatively high T (~800 °C).

Among the antisites theoretically assessed, i.e., Mo_S, S_{Mo}, $S2_{Mo}$, Mo_{S2}, E_{form} of the former two is anticipated to be smallest [5, 10, 11]. Yet, when dealing with MoS_2 grown under S-rich conditions, the E_{form} (~4 eV) of S_{Mo} emerges as resolutely the lowest [10]. The formation energy is further calculated to be drastically lowered at grain boundaries compared to the grain interior [23]. Accordingly, given the S-rich growth condition of the currently studied the MoS_2 layers, this would favor assignment of the ML1 signal to S_{Mo} defects.

This leads to the proposition that in the studied polycrystalline synthetic 2D MoS_2 layers, the grain boundary dislocation are the source of a large density of paramagnetic defects, that on comparative grounds, will unacceptably impair the layer's electrical and optoelectronic functionality.

Finally, when overviewing the results of the studied 4ML MoS_2 samples, we notice that the observed strong reduction (~4 times) with increasing grain size is in line with the measured drastic improvement in carrier mobility; It would indicate, not unexpectedly, that the grain boundaries with embedded (antisite) point defects are at the basis of the strong deterioration of the carrier mobility.

Conclusions

In conclusion, low-T ESR study has revealed that the grain boundaries in continuous large-area few-layer 2H MoS_2 films synthesized by sulfurization of Mo films have incorporated an excessive density of paramagnetic defects, a fact, as it appears, inherent to the preparation method applied. Occurring in densities of up to $\sim 3 \times 10^{12}$ cm^{-2} for 4 ML-thick MoS_2 films, on comparative grounds, these defects will inaptly impair and limit the charge carrier mobility and limit optoelectronic functionality. Led by stepwise elimination, the originating center is tentatively assigned to the S_{Mo} or $S2_{Mo}$ antisite, "inherently" associated with grain boundaries, an intrinsic structural defect of which the incorporation emerges as inherent to the growth method used. With respect to the fabrication method applied, the incorporation of

such type of defect in distinct quantities may perhaps not come as a surprise. The advanced hypothesis is to be subjected to verification by first-principle theoretical simulations able to reliably calculate g values of point defects in MoS_2 to sufficient accuracy.

Obviously, defects in 2D MoS_2 layers are generally detrimental for, and may cause undue large variations in, electrical and optical properties, and should thus be maximally suppressed or electrically inactivated, the more so for antisite-type defects. The currently gained information is expected to be of use on the road to refine and optimize the layer synthesis procedure, with the view to come to large area, continuous 2D transition metal dichalcogenide (TMD) layers of uniform device-grade quality throughout. As layered TDMs have very similar structures, the structural defect revealed in this work may be expected to surface in other 2D TDMs as well, e.g., WS_2, particularly when manufactured in a similar way.

Abbreviations

2D: Two dimensional; Cz: Czochralski; DB: Dangling bond; ESR: Electron spin resonance; ML: Monolayer; ADF: Annular Dark Field; STEM: Scanning transmission electron spectroscopy; TMD: Transition metal dichalcogenides

Acknowledgements

AS and SI are indebted to V. Tuts and P. De Greef for the preservation of electronic equipment.

Funding

This work was financially supported by the KU Leuven Research Fund (Project IDO/11/007) and the ERA-NET 2Dfun project (2D functional MX_2/graphene heterostructures) within the framework of the European Flagship Graphene.

Authors' Contributions

AS and SI completed the experiments, analyzed the data, and discussed the results in collaboration with VA and DC. AS and VA initiated the experiments and took care of the substrate preparation. DC, supported by IR, CH, and SD, carried out the film growth. AS and SI wrote the manuscript and revised it, with input from the other authors. All authors read and approved the final manuscript.

Competing Interests

The authors declare that they have no competing interests.

Publisher's Note

Author details

[1]Department of Physics and Astronomy, University of Leuven, 3001 Leuven, Belgium. [2]Imec, Kapeldreef 75, 3001 Leuven, Belgium.

Received: 28 November 2016 Accepted: 18 March 2017
Published online: 20 April 2017

References

1. Wang QH, Kalantar-Zadeh K, Kis A, Coleman JN, Strano MS (2012) Electonics and optoelectronics of two-dimensional transition metal dichalcogenides. Nat Nanotechnol 7:699–712
2. Ataca C, Sahin H, Ciraci S (2012) Stable, single-layer MX_2 transition metal oxides and dichalcogenides in a honey-comb-like structure. J Phys Chem C 116:8983
3. Butler SZ et al (2013) Progress, challenges, and opportunities in two-dimensional materials beyond graphene. ACS Nano 7:2898
4. Mak K, Lee C, Hone J, Shan J, Heinz T (2010) Atomically thin MoS_2: a new direct-gap semiconductor. Phys Rev Lett 105:136805
5. Hong J, Hu Z, Probert M, Li K, Lv D, Yang X, Gu L, Mao N, Feng Q, Xie L, Zhang J, Wu D, Zhang Z, Jin C, Ji W, Zhang X, Yuan J, Zhang Z (2015) Exploring atomic defects in molybdenum disulphide monolayers. Nat Commun 6:6293
6. Najmaei S, Yuan J, Zhang J, Ajayan P, Lou J (2015) Synthesis and defect investigation of two-dimensional molybdenum disulfide atomic layers. Acc Chem Res 48:31
7. Qui H, Xu T, Wang Z, Ren W, Nan H, Ni Z, Chen Q, Yuan S, Miao F, Song F, Long G, Shi Y, Sun L, Wang J, Wang X (2013) Hopping transport through defect-induced localaized states in molybdenum disulphide. Nat Commun 4:2642; Komsa H-P, Kotakoski J, Kurasch S, Lehtinen O, Kaiser U, Krasheninnikov AV (2012), Two-dimensional transition metal dichalcogenides under electron irradiation: defect production and doping. Phys. Rev. Lett. 109; 035503
8. Nyns L, Lisoni J, Van den Bosch G, Van Elshocht S, Van Houdt J (2014) Atomic layer deposition of scandium-based oxides. Phys Stat Sol A 211:409
9. Kaasbjerg K, Thygesen KS, Jacobsen KW (2012) Phono-limited mobility in n-type single-layer MoS_2 from first principles. Phys Rev B 85:115317
10. Komsa H-P, Krasheninnikov AV (2015) Native defects in bulk and monolayer MoS_2 from first principles. Phys Rev B 91:125304
11. Zhou W, Zou X, Najmaei S, Liu Z, Shi Y, Kong J, Lou J, Ajayan PM, Yakobson BI, Idrobo J-C (2013) Intrinsic structural defects in monomayer molybdenum disulfide. Nano Lett 13:2615
12. Santosh KC, Longo RC, Addou R, Wallace RM, Cho RM (2014) Impact of intrinsic atomic defects on the electronic structure of MoS_2 monolayers. Nanotechnology 25:375703
13. Haldar S, Vovusha H, Yadav MK, Eriksson O, Sanyal B (2015) Phys Rev B 92:235408
14. Zou X, Liu Y, Yakobson B (2013) Predicting dislocations and grain boundaries in two-dimensional metal-disulfides from first principles. Nano Lett 13:253
15. Liu D, Guo Y, Fang L, Robertson J (2013) Sufur vacancies in monolayer MoS_2 and its electrical contacts. Appl Phys Lett 103:183113
16. Addou R, Colombo L, Wallace RM (2015) Surface defects on natural MoS_2. ACS Appl Mater Interfaces 7:11921
17. Noh J-Y, Kim H, Kim Y-S (2014) Stability and electronic structures of native defects in single-layer MoS_2. Phys Rev B 89:205417
18. Keunen K, Stesmans A, Afanas'ev VV (2011) Inherent Si dangling bond defects at the thermal (110)Si/SiO_2 interface. Phys Rev B 84:085329
19. Chiappe D et al (2016) Controlled sulfurization process for the synthesis of large area MoS_2 films and MoS_2/WS_2 heterostructures. Adv Mater Interfaces 3:1500635
20. Weil JA, Bolton JR, Wertz JE (1994) Electron paramagnetic resonance; elementary theory and practical applications. Wiley and Sons, New York, p 535
21. Deroide B, Bensimon Y, Belougne P, Zanchetta JV (1991) Lineshapes of ESR signals and the nature of paramagnetic species in amorphous molybdenum sulfides. J Phys Chem Solids 52:853, ; Bensimon Y, Belougne P, Deroide B, Zanchetta JV, Giuntini JC, Henn F (1992), ESR study of influence of oxygen on molybdenum sulfides. J. Non-Cryst. Solids 149; 218
22. Hirth JP, Lothe J (1982) Theory of dislocations, 2nd edn. Wiley, New York
23. Yu ZG, Zhang Y-W, Yakobson BI (2015) An anomalous formation pathway for dislocation-sulfur vacancy complexes in polycrystalline monolayer MoS_2. Nano Lett 15:6855